Phys. Status Solidi C **14**, No. 1–2, 1600099 (2017) / **DOI** 10.1002/pssc.201600099

physica status solidi c
www.pss-c.com
current topics in solid state physics

Physicochemical effects of amino- or sulfur-functional groups onto SBA-15 sol-gel synthesized mesoporous ceramic material

Zulema Vargas-Osorio[1], Osmar Alejandro Chanes-Cuevas[1], Adriana Pérez-Soria[1], Manuel García-Hipolito[2], Octavio Alvarez-Fregoso[2], and Marco Antonio Alvarez-Perez[*,1]

[1] Laboratorio de Bioingeniería de Tejidos, División de Estudios de Posgrado e Investigación, Facultad de Odontología, UNAM, Circuito Exterior s/n. Cd. Universitaria, 04510 Coyoacán México, C. D. México
[2] Instituto de Investigaciones en Materiales, UNAM, Circuito de la Investigación Científica s/n. Cd. Universitaria, 04510 Coyoacán México, C. D. México

Received 23 June 2016, revised 12 September 2016, accepted 16 September 2016
Published online 4 October 2016

Keywords SBA-15, mesoporous materials, functionalization, cocondensation method, pore structure

[*] Corresponding author: e-mail marcoalv@unam.mx

SBA-15 mesoporous ceramics were synthesized by a sol-gel method with some modifications and functionalized with ethylenediamine or tetrasulfide groups and using a sequential washing approach of organic solvent mixtures. The effects of the functional groups onto the physicochemical properties were characterized using XRD, TG/DTA, FTIR, N_2 adsorption–desorption, TEM, SEM and NMR. These analyses showed that the SBA-15 ceramic synthesized at low temperature shows a flat two-dimensional hexagonal symmetry with pore diameters of 7.1 to 7.8 nm. In the meantime, the functionalized ethylenediamine SBA-15 presented a narrow pore-size distribution with diameter around 3.5 to 5.7 nm.

A different behavior was observed on the tetrasulfide SBA-15 showing a decrease in unit-cell parameter, in pore size (~ 2.5 nm) and an increase in pore wall size with loss in structural order and at high sulfur concentrations exhibited an amorphous structure. Results indicated that the lattice crystalline structure value of the SBA-15 increased due to the amino-functionalization process to a value of 13.48 nm respect to a value of 12.72 nm in SBA-15 and decreased to 10.12 nm as an effect of the sulfur-functionalization process, indicative of the effect of the amino and sulfur group into the well-ordered hexagonal mesoporous structure of SBA-15 ceramic materials.

1 Introduction Over the past few years, a family of mesoporous materials with high specific surface area and functionalized surface have received much interest and a great deal of attention because of their wide variety of scientific and technological applications in catalysts, adsorption, sensing, separation, optical devices, drug delivery and bone-tissue engineering [1–6]. Fundamental and applied research dealing with novel silica-based mesoporous materials as MCM-41, MCM-48 and SBA-15 aims to improve template-synthesis strategies, chemical modification of the porosity and surface of mesoporous materials in order to adjust to a more hydrophobic or hydrophilic character. In addition, to increase their reactivity it is needed to raise the covalent anchoring that provides great opportunities for immobilization of large catalytic species and catalytic conversion of diverse organic molecules that is of paramount importance in the pore engineering for their applications in the industry, engineering, environmental waste and biomedical areas [7–10].

SBA-15 is a mesoporous silica sieve with outstanding features including their uniform and highly ordered hexagonal pores. It has a narrow pore-size distribution of 20–300 Å and a tunable pore diameter between 5 and 15 nm, large pore volume (0.6–1.3 cm^3/g), high surface area (400–1000 m^2/g), high thermal stability and large thickness of the framework walls (3.1 to 8.4 nm), that open up the possibility for their functionalization [11–13].

The functionalization of SBA-15 is done by a cocondensation route where the organosilane group ((R'O)3SiR) reacts together with the silica precursor (TEOS) in the typical synthesis of SBA-15 that allows for a uniform homogeneous distribution of anchoring points on the silica

surface. Upon surfactant removal, the materials present a network of cavities within the silica framework that determines their physicochemical properties. However, the presence of remaining surfactant trapped within the pore structure would detrimentally affect the structure [14, 15]. Generally, two methods are used to remove the organic templates from these mesoporous materials, i.e., high-temperature calcination in air, or simple solvent washing (extraction). Moreover, when the mesoporous material is functionalized, only chemical removal by solvent washing could be used [11, 17, 34].

We propose new removal surfactant methods that could generate favorable changes on the surface properties of the mesoporous materials. Aiming at new applications and properties, much effort is being devoted to increase the number of available mesostructures by varying the templating agent and the synthesis conditions. The morphology of SBA-15 could be tuned in many ways for many applications, considering that the size, shape and order of the pores are the principal characteristics that determine the adsorption and delivery properties of these ceramics [18, 19]. Moreover, the morphology together with the functionalization play a key role in establishing the type of interactions that could occur in chemical, physical and biological systems [20–23].

In the present study, we have synthesized a mesoporous SBA-15 ceramic using an ethylenediamine (R1) or tetrasulfide groups (R2) as good candidates to be tested as functional groups. The influence of the synthesis and functionalization on the resulted mesoporous ceramics on their structural, textural, and physicochemical features were characterized by X-ray diffraction (XRD), N_2 adsorption/desorption (BET), Fourier transform infrared (FT-IR), nuclear magnetic resonance (NMR), scanning electron microscopy (SEM) and transmission electron microscopy (TEM).

2 Experimental The following reagents were used for the synthesis and extraction of the mesoporous materials: tetraethylorthosilicate (TEOS, $C_8H_{20}SiO_4$: 98%, Aldrich), N-[3 trimethoxysilyl) propyl]ethylenediamine ($C_8H_{22}N_2O_3Si$: 97%, Aldrich), bis[3-(triethoxysilyl)propyl] tetrasulfide ($C_{18}H_{42}O_6S_4Si_2$ ≥90%, Aldrich), polyoxyethylene-polyoxypropylene triblock copolymer (PEO_{20}-PPO_{70}-PEO_{20}, Pluronic® P123, Aldrich), hydrochloric acid (HCl: 36.5–38% WT, J.T. Baker), 2,2,4-trimethylpentane (isooctane, C_8H_{18} ≥ 99%, Tecsiquim), ethanol (C_2H_6O 9 QP, Morelos Co.) and acetone (C_3H_6O QP, Meyer Co.). The deionized water used (resistivity 18 MΩ m) was obtained from an ultrapure water system Milli-Q of Millipore.

2.1 Synthesis of SBA-15 ceramic material The SBA-15 materials were prepared following the method used by Vallet-Regí and coworkers [24], previously reported by Zhao et al. [25]. Some conditions were changed during the reaction, as described below. The SBA-15 material was carried out in a typical synthesis of: 8 g of triblock copolymer Pluronic P123, PEO_{20}-PPO_{70}-PEO_{20}, (as a structure-directing agent) were dissolved in a mixture of 276 mL of deionized water and 20.6 mL of reagent-grade hydrochloric acid (HCl: 37 wt%) and kept under magnetic stirring at 308 K. Once the surfactant was completely dissolved, 16.4 mL of TEOS 98% were added as a silica source to yield a molar composition of 1.0 SiO_2/0.017 P123/3.4 HCl/208 H_2O. After aging at 343 K for 24 h in a sealed crystal recipient, gels were collected by filtration, washed with deionized water and dried in air at 338 K for 24 h. Finally, dried powders were treated with new organic solvent method to remove the surfactant. For the functionalized SBA-15 materials prepared by the cocondensation method, the reagent was added drop wise during the first stage of the mesoporous matrix synthesis, after the addition of TEOS. The composition is shown in Table 1.

Table 1 Molar composition of the functionalized SBA-15 mesoporous materials.

Sample	TEOS (mL)	R1 (mL)	R2 (mL)	Molar composition
SBA-15E	16.40			1 TEOS
SBA-N1E	16.05	0.40		0.975 TEOS: 0.025 R1
SBA-S1E	16.05		0.92	0.975 TEOS: 0.025 R2
SBA-N2E	15.64	0.81		0.95 TEOS: 0.05 R1
SBA-S2E	15.64		1.84	0.95 TEOS: 0.05 R2
SBA-N3E	15.23	1.22		0.925 TEOS: 0.075 R1
SBA-S3E	15.23		2.76	0.925 TEOS: 0.075 R2

2.2 Surfactant-removal method The SBA-15 materials were subjected to several washing cycles in sequential form with different mixtures of organic solvents (50 mL mix/1g material). In each sequence, all the materials were left under vigorous magnetic stirring at 298 K for 6–8 h; after this process, they were collected by filtration and dried at 343 K for 2–4 h. The mixtures of organic solvents and its sequential application appear in Table 2.

Table 2 Organic solvent mixtures and proportions.

Sequence	Organic solvents	Proportion
1°	Isooctane:Ethanol	60:40
2°	Acetone:Water deionized	60:40
3°	Isoctane:Ethanol	60:40
4°	Water deionized:Acetone	60:40
5°	Water deionized	100

2.3 Characterizations of SBA-15 ceramic material The ordered mesoporous framework of the synthesized material was assessed by powder small angle X-ray diffraction (XRD) in a Siemens D-500 diffractometer operating with Cu Kα radiation (λ = 1.5405 Å) at 34 kV and 25 mA. The diffractograms were collected over the 0.5–8.0° 2Θ range with a step size of 0.02°, and a contact time of 5 s per step. The composition of the samples was analyzed by elemental microanalysis (CHNS) in a LECO

CHNS-932 thermoanalyzer. Characterization of SBA-15 and functionalized SBA-15 materials by thermogravimetric and differential thermal analyses (TG/DTA) were carried out between 313 K and 1273 K under a 100 ml/min argon flow and a heating rate of 10 K/min in a SDT Q600-TA thermobalance instruments. Fourier transform infrared (FTIR) spectra were recorded in an Alpha Bruker spectrometer in the attenuated total reflectance mode using the ATR method. The surface characterization of SBA-15 material was carried out by nitrogen adsorption/desorption analyses performed at 77 K using a Besorp-Mini of Bel-Japan Inc. The morphology and structure of SBA-15 and functionalized SBA-15 samples was characterized via transmission electron microscopy (JEOL JEM-1200EX microscope) and scanning electron microscopy (JEOL JSM-6701F microscope). The silicon environments were determined by solid-state ^{29}Si magic-angle spinning (MAS) nuclear magnetic resonance (NMR). The NMR spectra were obtained on a Bruker Advance 400 with spectral width of 32 kHz. A 4.0-mm rotor was used. The MAS speed was 5 kHz. ^{29}Si MAS NMR spectra were referenced to tetramethyl silane (TMS).

3 Results and discussion

The X-ray diffraction patterns of SBA-15 and the SBA-15 functionalized samples are displayed in Fig. 1. For the SBA-15E sample a highly ordered 2D hexagonal structure (P6mm) [26, 27] can be observed, that exhibits three well-resolved Bragg diffraction maxima (100), (110) and (200), associated with the conservation of the long-range order of the mesoporous frameworks. The unit-cell parameter (a_0) for the SBA-15 sample was calculated from the position of the (100) diffraction peak and has a value of about 12.72 nm. In contrast, the functionalized samples SBA-N1E and SBA-N2E showed a huge loss in the ordered structure, obtaining smooth peaks for the (100) position, from which a_0 was calculated, leading to an increased (a_0) parameter value of 13.48 and 13.40 nm, respectively. Thus, it could be deduced that an expansion of the unit cell might be caused by a partial dissolution of the mesopore frameworks that occurred from the decomposition of the Si-amino group on the surface of Si–OH. In the case of SBA-N3E, the material with the highest propyl ethylenediamine functionalization (R1), it showed a tenuous curvature; however, it was not possible to obtain a unit-cell parameter because the matrix possesses a disordered amorphous mesoporous structure [28, 29].

For the ceramics synthesized with the second reagent (propyl tetrasulfide (R2): SBA-SnE) a well-defined (100) diffraction peak is observed for the samples with the lowest functionalizing amount. A high presence of sulfur in the sample SBA-S3E confirms that the pore structure was totally disordered. However, (a_0) could be calculated for SBA-S1E an SBA-S2E, resulting in a parameter of 10.42 and 10.12 nm, respectively. This decreasing trend of the unit-cell parameter (a_0) might be caused by a grafting of the Si–OH groups with the sulfur groups onto the mesopores of the SBA-15. These results indicated that the lattice mesoporous structure value of the SBA-15 increased due to the amino-functionalization process to a value of 13.48 nm with respect to a value of 12.72 nm in SBA-15 and decreased to 10.12 nm as an effect of the sulfur-functionalization process. This is indicative of the effect of the amino and sulfur group into the well-ordered hexagonal mesoporous structure of SBA-15 ceramic material.

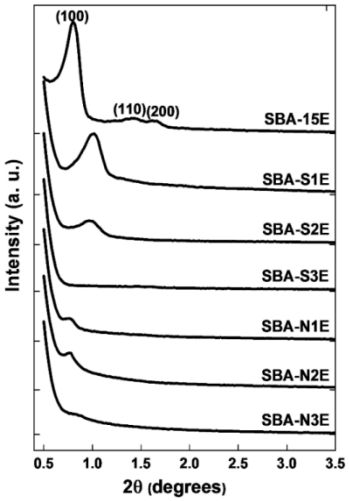

Figure 1 Small-angle XRD patterns of siliceous SBA-15 and functionalized materials.

The functionalized materials were analyzed by elemental chemical analysis to determine the content of nitrogen and sulfur in the mesoporous materials [26]. The experimental value is known and could be compared with the theoretical (initial weight %) value to understand their participation in the synthesis of the functionalized matrices. It could be assumed that all nitrogen derives from the amine groups present in the ethylenediamine molecule anchored in the mesoporous surface from each sample; at the same time all the sulfur could be expected to come from the tetrasulfide molecule and it is possible to obtain the percentage of functionalization of each material considering that all ethoxy and methoxy groups present in TEOS, R1 and R2 have been hydrolyzed during the reaction. The results are shown in Tables 3 and 4.

Note that in the case of the SBA-NnE materials the theoretical functionalization percentages are higher than those obtained experimentally, while for SBA-SnE samples the percentages are practically equal to the theoretical value. Both functional groups are Lewis bases, and so possess an electron pair capable to be shared to form a bond, which is why the ethylenediamine group in acid medium is protonated, this mean that the interaction between the chloride anion arising from the total dissociation of HCl has more affinity with the protonated amine than the protonated

Table 3 Comparison of theoretical and experimental functionalization of groups in the SBA-15 materials.

Samples	% Theoretical Functionalization	% Experimental Functionalization
SBA-N1E	2.5% R1	1.33% R1
SBA-N2E	5.0% R1	1.77% R1
SBA-N3E	7.5% R1	3.79% R1
SBA-S1E	2.5% R2	2.49% R2
SBA-S2E	5.0% R2	5.47% R2
SBA-S3E	7.5% R2	8.28% R2

Table 4 Comparison of theoretical and experimental weight percentage of the functional groups in the SBA-15 materials.

Samples	% Theoretical Weight		% Experimental Weight ± 5 W%	
	SiO_2	R1 or R2	SiO_2	R1 or R2
SBA-N1E	95.4	4.6	97.6	2.4
SBA-N2E	91.0	9.0	96.8	3.2
SBA-N3E	86.8	13.2	93.3	6.7
SBA-S1E	91.0	9.0	91.1	8.9
SBA-S2E	83.1	16.9	81.5	18.5
SBA-S3E	76.2	23.8	73.7	26.3

silanol group of the silica precursor, which directly affects the formation of the structure considering that one of the two proposed mechanisms and the most accepted by the scientific community for the formation of mesoporous silica materials is the organic–inorganic interactions of electrostatic type between the inorganic phase of silica and micellar aqueous medium phase. Additionally, this functional group has the property to interact with the deionized water and the other molecules present in the reaction through hydrogen bonds by perturbing the micellar medium phase during the formation of the hexagonal disposition. In the case of the tetrasulfide it is a weaker base than ethylenediamine and cannot interact through hydrogen bonds, accordingly the incorporation of this functional group into the surface is larger, although these present a limitation associated to the existing steric impediment of the bulky tetrasulfide group [30].

The FTIR spectrum of SBA-15E, SBA-N2E, SBA-S2E and their precursors (before surfactant's removal) are displayed in Figs. 2a–c. The three spectra show similar behavior before and after the surfactant was removed and present the same characteristic bands of the functional groups that form the mesoporous silica, however, it was not possible to observe the organic group of the functional molecule, due to the experimental percentages of functionalization being lower than the theoretical, hindering the appearance of their representative bands [7, 31, 32].

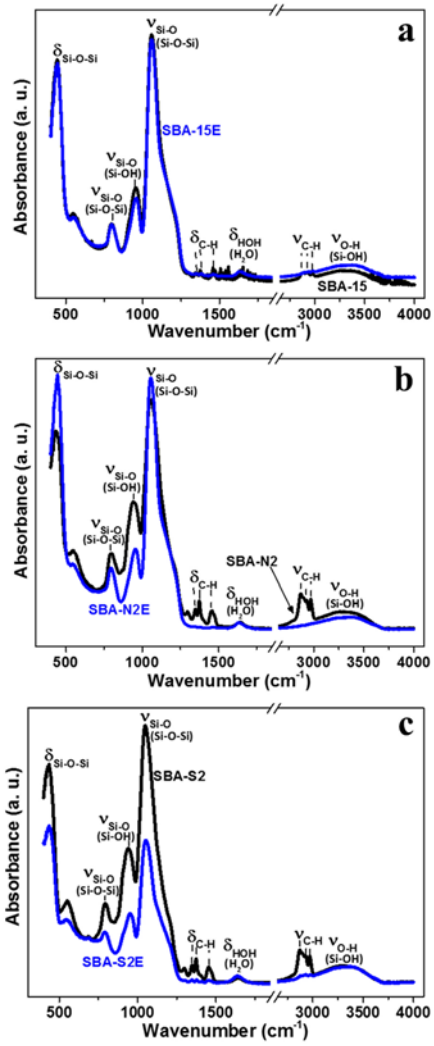

Figure 2 FTIR spectra of the: (a) SBA-15 and SBA-15E, (b) SBA-N2 and SBA-N2E, (c) SBA-S2 and SBA-S2E, mesoporous materials before and after removing the surfactant.

In general, the characteristic bands of a pure-silica material are observed; there is also evidence of the presence of a broad band corresponding to the vibration of silanol groups (ν_{Si-OH}) between 3000 and 3700 cm^{-1}. In addition, the high-intensity typical vibration bands of SiO_2 matrices was observed around 1055 cm^{-1} and 442 cm^{-1}, indicating the presence of siloxane groups corresponding to the asymmetric stretching (ν_{SiO}) and the bending vibrations (δ_{SiOSi}), respectively. Another characteristic weak band showed at 800 cm^{-1} relating to the symmetric stretching of Si–O (ν_{SiO}). The free silanol groups are represented by the peak at 941 cm^{-1} (ν_{SiOH}). Before surfactant removal, the vibration bands were observed approximately at 2900–3000 cm^{-1} stretching (ν_{CH}) and at 1350–1480 cm^{-1} torsion (δ_{CH}), characteristic of their hydrocarbon chains. After elimination, much of the surfactant was removed from the pores, and these bands have disappeared in Figs. 2a and b,

however, they are still present in the SBA-S2 sample with lower intensity (Fig. 2c). Finally, a weak vibration in the 1590–1700 cm^{-1} range can be ascribed to the adsorption of water in the material surface given by δ_{HOH} (H_2O).

The residual amount of surfactant in the samples has been determined by TGA/DTA analysis. Figure 3 shows a loss around 40–100 °C in all the cases that is related with the desorption process of physically adsorbed water or solvent trapped in the matrices after the surfactant's removal process. By DTA analysis, well-defined peaks are observed for the mesoporous materials SBA-15 type, which allow a determination of the temperature range at which surfactant disappears, starting at 170 °C and ending at 700 °C. The organic functionalized groups as well as the surfactant are lost in the same temperature range [33]. From the thermogravimetric analysis, a substantial reduction in the weight percentage of the organic material in all the matrices was clearly observed and these results are presented in Table 5. All samples show a first weight loss of 1–14% at temperatures lower than 100 °C, which correspond to the desorption of physically adsorbed water or acetone–ethanol. This is followed by a large weight loss of around 48–85% in the temperature range of 170–700 °C.

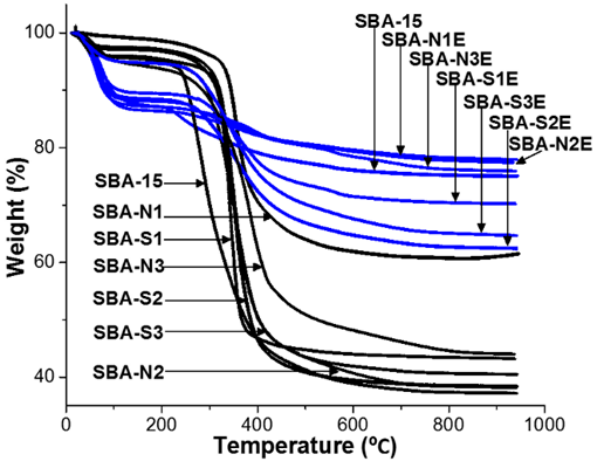

Figure 3 TGA of the mesoporous matrices before and after removing the surfactant.

The values of weight percentage removed expressed in Table 5 take into account only the surfactant loss. It is well known that subtracting the values of experimental weight percentage of the functional groups obtained by elemental chemical analysis from the remaining weight percentage calculated by TGA, will lead to an approximate value of the remaining amount of surfactant inside of each functionalized material.

The behavior is similar between each functional group; on average for the materials functionalized with reagent R1, the remaining surfactant weight percentage is around 12%, whereas in the synthesized materials with reagent R2 it is about 25%. These results may be related with the presence

Table 5 Weight percentage of removed organic matter.

Samples	% Weight T_i (170 °C)	% Weight T_f (700 °C)	% Organic Matter Weight (T_i–T_f)	% Weight Removed
SBA-15	98.98	60.98	38.00	69.26
SBA-15E	87.22	75.54	11.68	
SBA-N1	95.67	37.87	57.80	85.64
SBA-N1E	86.93	78.63	8.30	
SBA-S1	95.80	43.36	52.44	64.21
SBA-S1E	89.44	70.67	18.77	
SBA-N2	95.10	38.66	56.44	85.10
SBA-N2E	86.62	78.21	8.41	
SBA-S2	97.32	38.79	58.53	57.88
SBA-S2E	87.94	63.29	24.65	
SBA-N3	94.03	45.99	48.04	75.90
SBA-N3E	88.54	76.96	11.58	
SBA-S3	97.12	41.03	56.09	48.73
SBA-S3E	94.85	66.09	28.76	

of the ethylenediamine group in the surface making it more hydrophilic and allowing a higher penetration of the solvent in the interior of the pores than the tetrasulfide group that is less hydrophilic, anyway, the removal surfactant method is as effective as the other organic solvents methods used with the difference that only a smaller quantity of solvent is needed and the extraction was carried out easily at ambient temperature [34, 35].

Figure 4 shows the N_2 adsorption isotherms type-IV characteristic of the SBA-15 mesoporous materials. Their behavior is evident by the presence of a hysteresis cycle that shows that upon reaching the medium pressures a new adsorption process starts, corresponding to the capillary condensation in the mesoporous material [11, 24, 36, 38]. However, the hysteresis cycles are relatively different between the samples, while for SBA-15E they show the branches of parallel adsorption and desorption indicating the existence of cylindrical mesoporous geometry. For the rest of the samples it is observed that the adsorption and desorption mechanisms represent different porous arrangements [15, 31, 43, 44].

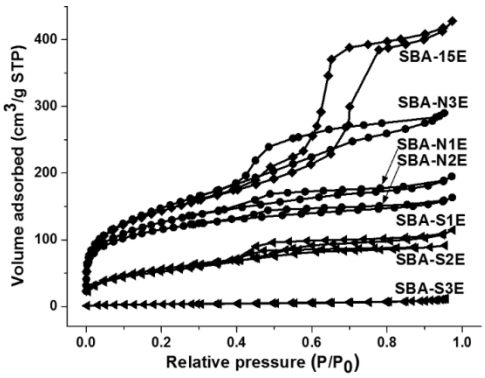

Figure 4 Nitrogen adsorption–desorption isotherms of the mesoporous matrices.

In Fig. 5 are indicated the N_2 adsorption isotherms in an amplified version. The SBA-S1E and SBA-S2E present a H2-type hysteresis cycle, which means they have a pore-size distribution and morphology that is not very well defined [37, 38]. In any case, the hysteresis loop corresponding to a pore-size distribution is broader than the hysteresis loop present in the H1 type, agreeing with the results obtained in XRD, where a loss in the ordered 2D hexagonal structure was observed. The SBA-S3E is well represented by the H3 type; this type of cycle, unlike the H1 and H2 types does not present a limited adsorption platform at relatively high pressure conditions close to the saturation pressure. It is formed by laminar particles and flexible pores with slit morphology [44]. The samples SBA-N1E, SBA-N2E and SBA-N3E are represented by the H4-type hysteresis cycle, which exhibits small pores sizes.

The evaluation of the adsorption and desorption branches of the isotherms and the hysteresis between them using the BJH method [38], reveals information about the SBA-15 mesoporous samples like size, volume, and surface area. The results are shown in Table 6.

Table 6 Textural values of mesoporous matrices.

Samples	S_{BET} (m^2/g)	V_p (cm^3/g)	D_{BJH} (nm)	a_0 (nm)	T_{wall} (nm)
SBA-15E	426.95	0.66	7.1	12.72	5.63
SBA-N1E	405.80	0.30	3.5	13.48	9.98
SBA-S1E	183.34	0.17	3.7	10.12	6.41
SBA-N2E	370.28	0.25	>2.5	13.40	10.67
SBA-S2E	195.61	0.14	>2.5	10.42	7.52
SBA-N3E	501.31	0.44	~2.5	---	---
SBA-S3E	11.58	0.05	≤2.0	---	---

From the adjacent mesoporous matrix the thickness of the siliceous wall (t_{wall}) can be deduced by subtracting the value of pore diameter (D_{BJH}) from the value of the lattice parameter, (a_0), obtained by XRD [38, 44]. The pore diameter distribution of the mesoporous matrices is presented in Fig. 6.

When the pore diameter (D_{BJH}) appears to be smaller than 2.5 nm, it is because this method approximates to the real value only when they have an ordered pore arrangement [16]. The synthesized materials have asymmetric pore systems of various morphologies and sizes, therefore the obtained diameters are far from the real value attributed to a poor assembly of the mesostructures at high amino and high sulfur groups. The aspects of the changes of the hysteresis loop, the shift of the inflection position toward a lower P/P_0 ranging from 0.37 to 0.96 and the reduced pore size for functionalized SBA-15 indicates that a functionalization might induce both pore contraction and partial collapses or pore blockage for SBA-15 sample [43, 44].

Pore contraction could be attributed to an increased amount of the incorporated organic functional group within the pores [11]. The results shown in Table 5 indicated that

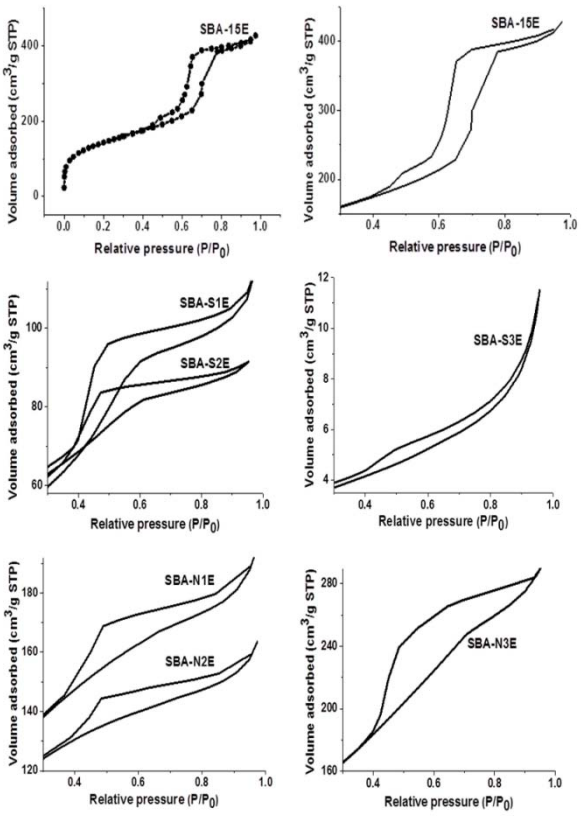

Figure 5 Nitrogen adsorption–desorption isotherms in amplified version: (a) SBA-15E (H1), (b) SBA-S1E, SBA-S2E, (c) SBA-N1E, SBA-N2E, (d) SBA-N3E and (e) SBA-S3E samples.

the functionalized samples had a smaller pore size (~2.5 nm) and thicker pore walls (~ 10.5 nm) when compared with SBA-15 sample. As expected for R1 and R2 functionalized SBA-15 samples, the BET surface area, the BJH pore sizes and pore volumes of the materials decrease gradually with the increase of R1 and R2 content as an effect of the occupation of large organic groups in the pore channels, while the wall thickness of the materials increases with R1 and R2 content [15].

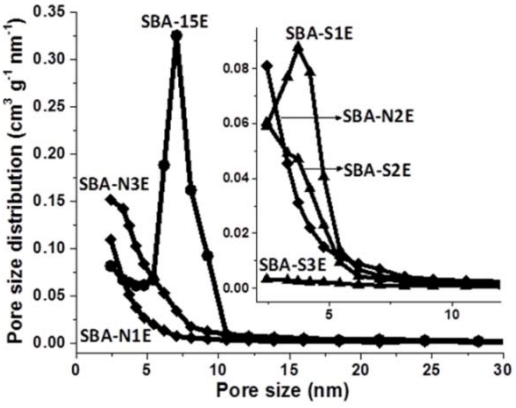

Figure 6 Pore-size distribution of the mesoporous matrices.

For instance, SBA-15 material exhibited characteristics values of surface area of 426.95 (m^2/g), pore volume (0.66 cm^3/g), pore diameter (7.1 nm), lattice parameter: a_0= 12.72 nm and a pore wall size of 5.63 nm. Meanwhile, samples SBA-N1E, SBA-N2E and SBA-N3E showed surface areas of 405.80; 370.28 and 501.31 (m^2/g), pore volumes of 0.30; 0.25 and 0.44 (cm^3/g), pore diameters of 3.5; 2.5 and ≤ 2.0 nm, lattice parameters a_0 of: 13.48, 13.40 nm and amorphous with an amine R1 content of 1.33: 1.77 and 3.79 wt% with increased pore wall size of: 9.98, 10.67 nm and undetermined pore wall size value, respectively, while samples SBA-S1E, SBA-S2E and SBA-S3E presented surface areas of 183.34; 195.61 and 11.58 (m^2/g), pore volumes of 0.17; 0.14 and 0.10 (cm^3/g), pore diameters of 3.7; ~2.5 and ≤2.0 nm, lattice parameters a_0 of 10.12; 10.42 nm and amorphous with a sulfide R2 content of 2.49; 5.47 and 8.28 wt% with increased pore wall size of: 6.41, 7.52 nm and undetermined pore wall size value, respectively.

Scanning electron microscopy allows a comparison of the morphology between the SBA-15E (Fig. 7a) and SBA-S1E (Fig. 7b) matrices. Figure 7a, shows long filaments that represent the capillaries with open hexagonal shape at both ends, characteristic of this type of mesoporous matrices. However, when the percentage of functionalization increases, the distortion in the size and morphology of the filaments becomes evident, as shown in the case of SBA-S2E sample with a not well-defined structure (Fig. 7c). In the SBA-N1E micrograph (Fig. 7d), the morphology is similar to a corrugated paper sheet with pores formed between the grooves that match with the information obtained by BET. This material possesses a H4-type hysteresis cycle, which tends to form pores by stacking between sheets.

The SBA-N2E (Fig. 7e) present two morphology types: particle clusters and microspheres [28, 39–41]; the SBA-N3E (Fig. 7f) also shows particles accumulation. Both materials have similarities with the structure of the bioglasses [42], which is confirmed by XRD showing a fairly amorphous component. The microspheres may have formed by attempting to adopt an intermediate morphology between the sheets that has the SBA-N1E sample and the particle clusters of SBA-N3E sample. Finally, the SBA-S3E sample (Fig. 7g) corresponds to an amorphous material [29], which possesses aggregates and elongated particles like rods smaller than those obtained in the SBA-N2E sample.

The presence and configuration of the porous systems of these materials could be seen conveniently using transmission electron microscopy to describe the ordered and disordered systems, respectively. Evidently, the SBA-N1E and SBA-N2E materials have the hexagonal disposition of the pores, whose longitudinal direction is perpendicular to the plane of the TEM image. In Fig. 8a it can be observed the hexagonal structure with well-ordered pores and with equal size (~7.8 ±0.4 nm). In the TEM image in Fig. 8b corresponding to the sample SBA-N2E, a noticeable decrease in the structural order similar to the silica mesoporous particles reported in the literature can be observed and in the inset the disordered pores with different sizes (~5.7 ±0.4 nm) and high distortions are illustrated.

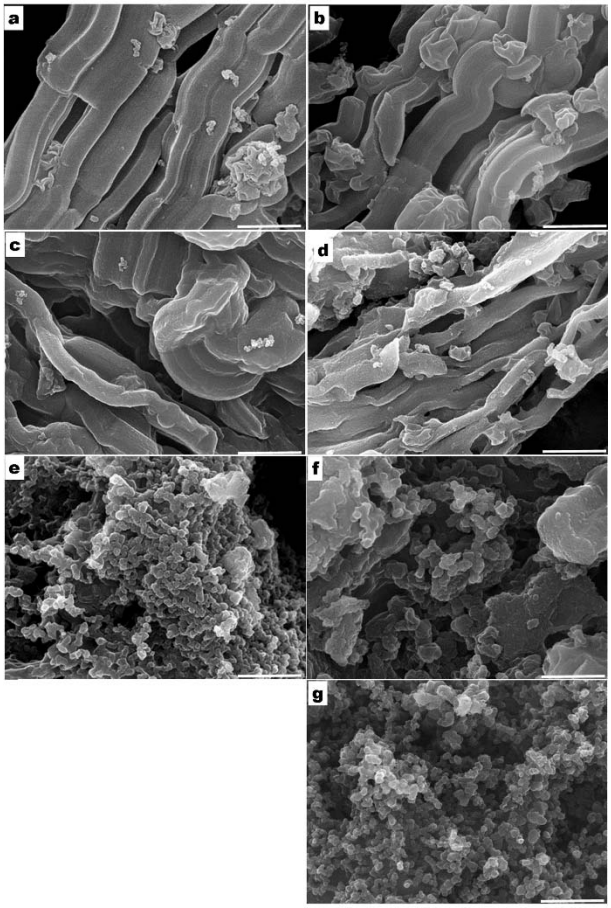

Figure 7 SEM micrographs of siliceous SBA-15 and functionalized materials: (a) SBA-15E, (b) SBA-S1E, (c) SBA-S2E, (d) SBA-N1E, (e) SBA-N2E, (f) SBA-N3E, and (g) SBA-S3E. Bar = 1 μm.

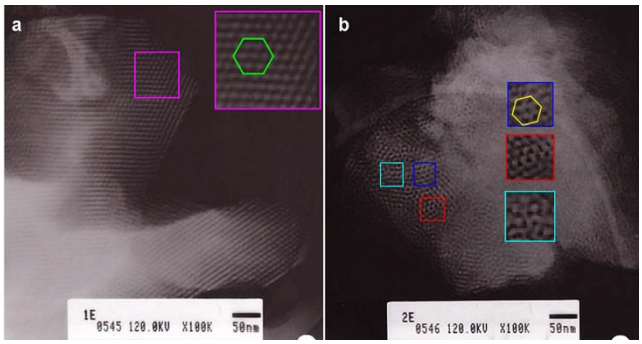

Figure 8 TEM micrographs of siliceous SBA-15 (a) and functionalized materials (b).

TEM images of the SBA-15 sample and functionalized materials are illustrated in Fig. 9. Figures 9a–c show well-ordered and clear one-dimensional channel structures along all the SBA-15, SBA-N1E and SBA-S1E materials. Clear areas corresponding to the empty pores (~7.3 ±0.4 nm) and darker regions (contrast) correspond to pores walls (~7.2 ±0.4 nm). All the images show the longitudinal arrangement of mesopores characteristics of SAB-15 materials. Figures 9d–f show semi-ordered pore structures with increased pore wall thickness with respect to Figs. 9a–c.

Figure 9g corresponds to the sample with the highest concentration of tetrasulfide groups does not present any indication of contrast due to the pore structure as corresponds to a disordered and amorphous material due to the functional tetrasulfide groups are practically filling up the pores as well as covering the outer surface of the particles.

Figure 10 represents the ^{29}Si CP-MAS NRM spectra of SBA-15E sample and the functionalized samples. Three up-field resonance signals concerning to the siloxane centers Q^4 ($\delta = -111$ ppm), Q^3 ($\delta = -101$ ppm), and Q^2 ($\delta = -92$ ppm) can be seen [14, 24]. Similarities between samples of each functionalized group are observed; the ratio of the peak intensity of Q^3:Q^4 for samples SBA-NnE is higher than that for samples SBA-SnE, indicating that for SBA-NnE samples the ethylendiamine groups are covalently grafted to the silica matrix through three siloxane (Si–O–Si) bridging bonds. For the functionalized materials with tetrasulfide group (SBA-SnE) it is observed a lower condensation of the silicate network by the presence of a higher intensity Q^3 peak than the Q^4 and also by the contribution of the Q^2 silica site. The presence of tetrasulfide groups anchored by both sides of the molecule to the silica walls greatly affects the condensation of the silanol groups during the reaction.

Moreover, a mesoporous ordered structure is maintained, which is consistent with the results obtained by BET and XRD, having surface areas lower than those shown by the SBA-NnE materials, while simultaneously presented a well-resolved Bragg diffraction maxima (100). A high amount of silanol groups in their surface could be favorable for their bioactivity, because it is known that the presence of silanol groups on the bioglass surface contribute largely to their excellent bioactivity. The SBA-S3E material possesses free silanols groups and the material is practically amorphous with poor textural properties due to a higher amount of the functional group.

The experimental characterization results indicate that the main difference between ethylenediamine and tetrasulfide functionalized mesoporous materials with respect to SBA-15 material consisted of the increases of the lattice parameter of the SBA-15 material due to the effect of the ethylenediamine from 12.72 nm to 13.48 nm and the decreases of the lattice parameter of the SBA-15 material due to the effect of the tetrasulfide from 12.72 nm to 10.12 nm values.

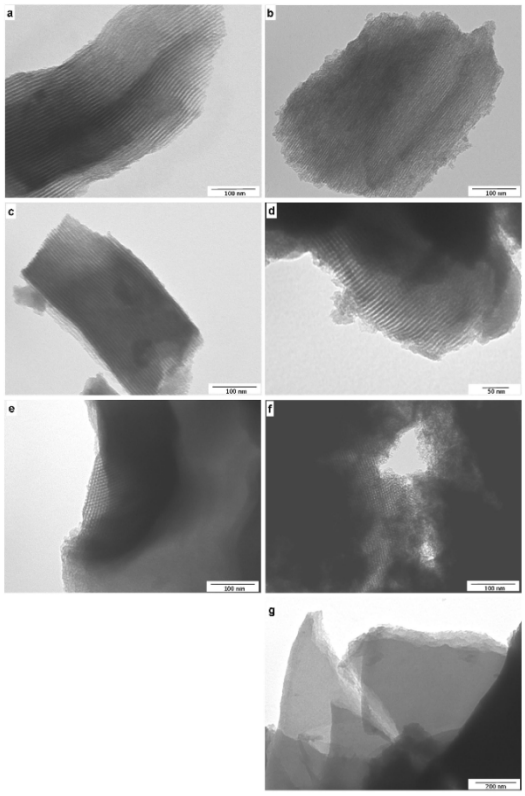

Figure 9 TEM images of the SBA-15 and functionalized materials showing the characteristic contrast of pores (clear-light) and pores walls (dark): (a) SBA-15E, (b) SBA-N1E, (c) SBA-S1E, (d) SBA-N2E, (e) SBA-S2E, (f) SBA-N3E and (g) SBA-S3E.

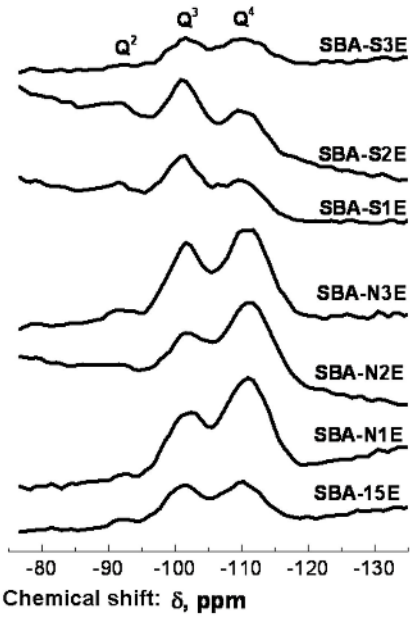

Figure 10 ^{29}Si CP-MAS NRM spectra of SBA-15 and functionalized materials.

4 Conclusions The SBA-15 material retained its distinctive characteristics and presented good textural properties, in spite of being synthesized at lower temperature than the conventional one. A reduced order of homogeneity of the pores was observed in the SBA-S1E and SBA-S2E functionalized samples that have a bulky tetrasulfide group. These materials preserve a high concentration of silanol groups (Si–OH) on their surface due to the existence of structural defects so it could carry out a second functionalization by postsynthesis method (impregnation technique), which would increase their reactivity and to change their properties. For the functionalized materials with a high concentration of ethylenediamine groups, mesoporous amorphous structures were obtained, having good textural properties that make them potential candidates to be used as an absorber of pollutant in water waste materials and a CO_2 absorber as they might avoid the limitations for pure mesoporous SiO_2 (low reactivity). Finally, the surfactant removal method used turned out to be easy to perform, cheap, requires no special equipment, with good results comparable to those reported in the literature. In summary, well-ordered surface functionalized mesoporous silica SBA-15 ceramic was readily synthesized using a novel and effective method at low temperatures and included the following advantages: preventing the destruction of the mesoporous structure at low concentration of functional groups; providing high functional behavior and could be high loading of amino (3.79 wt%) and sulfur (8.28 wt%) groups on the SBA-15 sample with the cost of the amorphization of the mesoporous structure.

Acknowledgements The authors wish to thank Omar Novelo Peralta, Raul Reyes Ortíz, Adriana Cruz Tejeda and Gerardo Cedillo Valverde from IIM-UNAM, for their technical assistance. ZVO wishes to thank CONACYT for a doctoral scholarship during the course of this study. This research was financially supported by funds from DGAPA-UNAM: PAPIIT IN210815.

References

[1] H. R. Chen, J. L. Shi, Y. S. Li, J. N. Yan, Z. L. Hua, H. G. Chen, and D. S. Yan, Adv. Mater. **15**, 1078 (2003).
[2] J. L. Gu, J. L. Shi, G. J. You, L. M. Xiong, S. X. Qian, Z. L. Hua, and H. G. Chen, Adv. Mater. **17**, 557 (2005).
[3] M. Vallet-Regí, A. Ramila, R.P. del Real, and J. Pérez-Pariente, Chem. Mater. **13**, 308 (2001).
[4] Y. F. Zhu, J. L. Shi, W. H. Shen, X. P. Dong, and J. W. Feng, Angew. Chem. Int. Ed. Engl. **44**, 5083 (2005).
[5] M. Vallet-Regí and E. Ruiz-Hernández, Adv. Mater. **23**, 5177 (2011).
[6] N. Shadjou and M. Hasanzadeha, Mater. Sci. Eng. C **55**, 401(2015).
[7] Y. Sánchez-Vicente, C. Pando, M. Cortijo, and A. Cabañas, Micropor. Mesopor. Mater. **193**, 145 (2014).
[8] L. Treccani, T.Y. Klein, F. Meder, K. Pardun, and K. Rezwan, Acta Biomater. **9**(7), 7115 (2013).
[9] R. Sanz, G. Calleja, A. Arencibia, and E. S. Sanz-Pérez, Micropor. Mesopor. Mater. **158,** 309 (2012).
[10] K. Tak-Hyun, J. Min, and J. K. Park, Micropor. Mesopor. Mater. **108,** 22 (2008).
[11] J.P. Thielemann, F. Girgsdies, R. Schlögl, and Ch. Hess, Beilstein J. Nanotechnol. **2,** 110 (2011).
[12] Y. Wang, F. Zhang, J. Ren, Ch. Li, X. Liu, Y. Guo, and G. Lu, Mater. Chem. Phys. **115,** 649 (2009).
[13] J. Ruan, T. Kjellman, Y. Sakamoto, and V. Alfredsson, Langmuir **28,** 11567 (2012).
[14] D. Margolese, J. A. Melero, S. C. Christiansen, B. F. Chmelka, and G. D. Stucky, Chem. Mater. **12,** 2448 (2000).
[15] X. Wang, C. C. Jerry Chang, T. Yao-Hung, and S. Cheng, Micropor. Mesopor. Mater. **95,** 57 (2006).
[16] M. L. Ojeda, J. M. Esparza, A. Campero, S. Cordero, I. Kornhauser, and F. Rojas, Phys. Chem. Chem. Phys. **5,** 1859 (2003).
[17] Y. K. Bae and O. H. Han, Micropor. Mesopor. Mater. **106**(1-3), 304 (2007).
[18] L. F. Gutiérrez, S. Hamoudi, and K. Belkacemi, Catalysts **1**(1), 97 (2011).
[19] E.S. Sanz-Pérez, M. Olivares-Marín, A. Arencibia, R. Sanz, G. Calleja, and M. Maroto-Valer, Int. J. Greenh. Gas Cont. **17,** 366 (2013).
[20] S. Parambadath, A. Mathew, M. J. Barnabas, and Ch. S. Ha, Micropor. Mesopor. Mater. **215,** 67 (2015).
[21] D. Zhang and J. H. Li, Chin. Sci. Bull. **58**(8), 879 (2013).
[22] A. Tewodros and T. Zhimin, Chem. Res. Toxic. **25**(11), 2265 (2012).
[23] T. W. Kim, II. Slowing, P. W. Chung, and V. S. Lin, ACS Nano. **5**(1), 360 (2011).
[24] M. Colilla, F. Balas, M. Manzano, and M. Vallet-Regí, Chem. Mater. **19**(13), 3099 (2007).
[25] D. Zhao, J. Feng, Q. Huo, N. Melosh, G. H. Fredrickson, B. F. Chmelka, and G. D. Stucky, Science **279,** 548 (1998).
[26] A. L. Doadrio, J. M. Sánchez-Montero, J. C. Doadrio, A. J. Salinas, and M. Vallet-Regí, Micropor. Mesopor. Mater. **195,** 43 (2014).
[27] Y. Wang, F. Zhang, J. Ren, C. Li, X. Liu, Y. Guo, and G. Lu, Mater. Chem. Phys. **115,** 649 (2009)
[28] J. Su, L. Cao, B. Yu, S. Song, X. Liu, Z. Wang, and M. Li, Internat. J. Nanomed. **7,** 2547 (2012).
[29] E. Rezabeigi, P. M. Wood-Adams, and R. L. Drew, Mater. Sci. Eng. C **40,** 248 (2014).
[30] F. Hoffmann, M. Cornelius, J. Morell, and M. Fröba, Angew. Chem. Int. Ed. **45,** 3216 (2006).
[31] A. López-Noriega, D. Arcos, and M. Vallet-Regí, Chem. **16**, 10879 (2010).
[32] A. El Kadib, P. Hesemann, K. Molvinger, J. Brandner, C. Biolley, G. Philippe, J. J. E. Moreau, and D. Brunel, J. Am. Chem. Soc. **131,** 2882 (2009).
[33] H. Zhu, C. Hu, F. Zhang, X. Feng, J. Li, and T. Liu, J. Chen, J. Zhang, Mater. Sci. Eng. C **42,** 22 (2014).
[34] R. Van Grieken, G. Calleja, G. D. Stucky, J. A. Melero, R. A. García, and J. Iglesias, Langmuir **19**(9), 3966 (2003).
[35] W. Whitnall, T. Asefa, and G. A. Ozin, Adv. Funct. Mater. **15,** 1696 (2005).
[36] R. M. Grudzien, B. E. Grabicka, R. Felix, and M. Jaroniec, Adsorption **13,** 323 (2007).
[37] M. Colilla, M. Manzano, I. Izquierdo-Barba, M. Vallet-Regí, C. Boissiére, and C. Sanchez, Chem. Mater. **22,** 1821 (2010).

[38] E. P. Barrett, L. G. Joyner, and P. P. Halenda, J. Am. Chem. Soc. **73,** 373 (1951).
[39] L. Gómez, E. Pabón Gélves, B. L. López, and A. Ramírez Vélez, DYNA **77,** 49 (2010).
[40] V. Chokkalingam, B. Weidenhof, M. Krämer, S. Herminghaus, R. Seemann, and W. F. Maier, Chem. Phys. Chem. **11,** 2091 (2010).
[41] V. Gascón, I. Díaz, C. Márquez-Álvarez, and R. M. Blanco, Molecules **19,** 7057 (2014).
[42] Z. Zhang, L. Zhang, C. Zhang, and W. Zhang, Talanta **119**, 485 (2014).
[43] S. M. Chong and X. S. Zhao, J. Phys. Chem. B **107,** 12650 (2003).
[44] M. Thommes, Physical Adsorption Characterization of Ordered and Amorphous Mesoporouos Materials, in: Nanoporous Materials, edited by G. Q. Lu and X. S. Zhao, (Sci. Eng. I. C. Press, Oxford, 2004).

